ACS APPLIED POLYMER MATERIALS

pubs.acs.org/acsapm

Article

Fluorescent Polyethylene by In Situ Facile Synthesis of Carbon Quantum Dots Facilitated by Silica Nanoparticle Agglomerates

Sida Yin, Joost Duvigneau,* and G. Julius Vancso*

Cite This: *ACS Appl. Polym. Mater.* 2021, 3, 5517−5526

Read Online

ACCESS | Metrics & More | Article Recommendations | Supporting Information

ABSTRACT: We describe an in situ facile synthetic approach to prepare carbon quantum dot (CQD) fluorescent markers (FMs) for polyethylene (PE) in the presence of agglomerated silica nanoparticles (SiO_2 NPs) under mild reaction conditions. First SiO_2 NPs, prepared by the Stöber method, were dispersed in toluene. This dispersion was added to a PE solution in toluene. After heating (either in air or under Ar) a fluorescent mixture was obtained. After drying, PE films were obtained by compression molding, which showed strong blue fluorescence, attributed to CQDs. SiO_2 NPs loading values varied between 0.5 and 4 wt %. Subsequent to isolation, the fluorescent CQDs were characterized by TEM, UV−vis, and fluorescence spectroscopy. TEM imaging unveiled a lattice spacing value of 0.21 nm of the isolated fluorescent particles which is typical for (100) graphite plane lattice spacing in CQDs. UV spectroscopy and fluorescence measurements show characteristic absorption and excitation spectra for the aromatic core and oxidized surface defects typically observed for CQDs. The emission maximum for PE/CQD samples increased from 394 to 408 nm when the reaction temperature was decreased from 110 to 90 °C, which is attributed to increasing oxygen content in the reaction mixture upon decreasing the reaction temperature. When the reaction was performed under Ar, the PE/CQD samples emitted in the ultraviolet region (286 nm). Finally, we demonstrated that PE samples marked with CQDs can be easily visually identified upon irradiating with 367 nm light. Thus, the marked PE can be used, for example, as a labeling ingredient in master batches for component identification and in recycling.

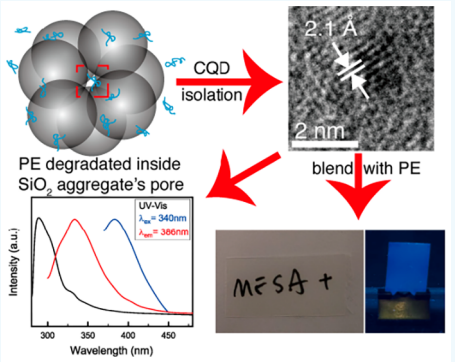

KEYWORDS: *polyethylene, fluorescence, silica nanoparticles, carbon quantum dots, optical markers, plastic sorting*

INTRODUCTION

To decrease the environmental impact of plastic waste and consumption of fossil resources employed in the production of plastics, recycling plastic waste is an essential practice. However, plastic sorting efficiency and component identification remain a technological challenge.[1−3] To increase the recycling rate for plastic waste, one needs to improve the sorting accuracy and speed. To this end, adding fluorescent markers (FMs) to enable high-efficiency sorting is one of the most promising approaches.

Currently, there are three main approaches to plastic waste management. These are landfilling, incineration, and chemical/mechanical recycling.[2] In general, plastic waste streams are treated with other municipal waste streams for landfilling and incineration. More than 80% of the waste plastic is disposed in the landfill.[2] Because of plastics' usually high resistance to degradation, it can take more than 50 years for a piece of plastic to degrade after being buried.[4,5] Degradation of landfilled plastic waste can damage the environment by, for example, releasing large amounts of greenhouse gases (CO_2), accelerating global warming, and forming microplastics/nanoplastics that may eventually accumulate in humans.[6,7] Besides these environmental concerns, landfilling is getting increasingly expensive in highly populated areas, like in Western Europe and in Southern China.[8] Incineration is also a standard method for plastic waste management.[2] Its most significant advantages are that upon incineration the waste volume is reduced and, simultaneously, the heat of combustion can be used for electricity generation. In 2015, ∼12% of the global plastic waste was incinerated.[9] However, the toxic gases released by incineration pose a significant health and environmental concern, especially when the incineration plants are operated in densely populated areas.[10] Furthermore, the incineration of plastic waste is accompanied by a relatively high CO_2 emission. Incineration of 1 kg of plastic waste can release up to 4.6 kg of CO_2, which for 1 kg of municipal solid waste (MSW) is only 1.2 kg.[11] Typically, MSW contains ∼10−12% of plastic. Thus, sorting plastic waste from MSW before

Received: July 8, 2021
Accepted: September 24, 2021
Published: October 22, 2021

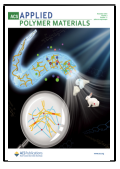

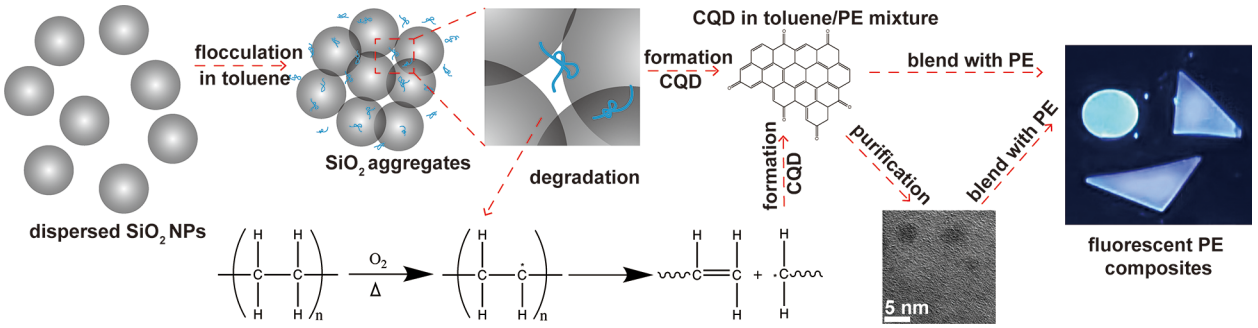

Figure 1. Schematic of CQD formation through thermal PE degradation inside the cavities/pores of silica nanoparticle aggregates. The method does not require extensive particle purification; upon removing the solvent, the particles are readily used as FMs in PE.

incineration will substantially decrease greenhouse gas emissions.[10]

Compared to landfilling and incineration, recycling is an eco-friendlier way to deal with plastic waste.[11−13] Recycling plastic reduces the above-mentioned environmental issues and decreases the required amount of fossil fuel to produce new plastic by reducing the demand for virgin materials. It is widely accepted that recycling plastics is an essential step toward creating a circular economy.[14] There are two main approaches for recycling plastics, that is, by using chemical or mechanical methods.[3] Depending on the composition of the plastics to recycle, each method has its strengths and weaknesses.[1]

The sorting of plastic waste typically consists of three steps.[1] First, Fourier transform near-infrared (FTNR) spectroscopy and a color recognition camera are used to presort various plastic types from waste streams. The second step consists of milling the plastic waste into small pieces and removing the nonplastic residuals. The final step is to further sort the milled plastics by type. Various techniques are in place for sorting plastic waste streams, like sink/float separation,[15] electrostatic separation,[16] air elutriation,[17] froth flotation,[18] and selective degradation.[19] Each of the above-mentioned techniques has its strengths and weaknesses; for more details, the interested reader is directed to ref 20.

The use of FMs, as an accurate and cost-effective approach to identify and sort specific polymers from plastic waste streams, has received considerable attention in recent years.[21−25] FMs can be incorporated in polymer matrices via masterbatches, e.g., by extrusion or injection molding. They can even be applied as a thin fluorescent coating onto the finished plastic products or intermediates.[26,27] For instance, Massardier et al. reported the incorporation of 0.1 wt % of lanthanide complex particles into a polypropylene (PP) matrix under a high shear rate (N = 800 rpm) to prepare a fluorescent polypropylene that is detectable with UV-ray fluorescence spectrometry within 10 ms.[23] Langhals et al. reported using organic dyes, that is, perylene ester, perylene carboxylic bisimide, and terylene carboxylic bisimide FMs, to identify polymers by measuring the time constant of autofluorescence decay values.[25] They also demonstrated that the polymer type (styrene−polyacrylonitrile copolymer, polyoxymethylene, or polyamide) alters the fluorescence lifetime values of the incorporated markers. This observation opened the path toward using the difference in the time constant values of the autofluorescence decay in sorting of different types of plastics. Recently, Woidasky et al. reported adding oxide crystals, doped with rare earth elements, as upconversion inorganic FMs to the polymer matrix for marking and identification.[28] By utilizing the upconversion fluorescence of the FMs, the authors were able to generate photoluminescence (PL) in the visible light range upon near-IR (NIR) excitation and, as such, eliminate the influence of background emission from plastics and additives.

Despite promises, there are numerous open challenges when considering the use of fluorescent particles/dyes at industrially relevant scales. For instance, fluorescent particles/dyes usually suffer from high cost, toxicity, and poor photostability.[29−32] These drawbacks currently limit their use as FM-labeled plastics on a large scale. Thus, if progress is to be made in this area, additional efforts are needed. Keeping this in mind, we decided to tackle the problem of loading PE by carbon quantum dots (hereinafter CQDs) and explored facile reaction routes to obtain fluorescent labeled PE.

CQDs are considered as a viable alternative for fluorescent dyes and inorganic QDs because of their low toxicity, low cost, good solubility, and high photostability.[33] A variety of techniques have been deployed to synthesize CQDs. These methods can be classified into two categories, that is, top-down and bottom-up approaches.[34−36]

The "top-down" method usually involves chemical, electrochemical, and physical approaches to break down large carbon-based materials, i.e. carbon soot, carbon nanotubes, graphite, etc.[37,38] The "bottom-up" approach typically utilizes solvothermal/hydrothermal carbonization, laser ablation, electrochemical oxidation, microwave irradiation, or pyrolysis to grow CQDs from organic molecules.[39] Many organic compounds have been reported to be used to synthesize CQDs via the bottom-up method, for instance, polybasic acid, glucose, sucrose, glycol, glycerol, and chitosan.[40−44] Among the techniques used to synthesize CQDs, solvothermal/hydrothermal carbonization is considered one of the simplest, most direct, and most efficient pathways.[43] However, the complicated chemical reactions, time-consuming purification, and harsh synthesis conditions pose serious challenges for large-scale applications.[36,45]

In this paper we introduce a facile "bottom-up" route that uses silica nanoparticles (SiO_2 NPs) as enablers to fabricate fluorescent CQDs from polyethylene (PE). The reaction scheme is captured in Figure 1. One of the most beneficial features of this route is that, upon removal of the solvent, the CQD, silica, and PE mixture is present in a concentrated FM blend, which can be used as a masterbatch to add to (virgin) PE. Hence, extensive and costly CQD collection and purification are not required. This opens new avenues to the widespread applicability of CQDs as FM for plastic waste

https://doi.org/10.1021/acsapm.1c00821
ACS Appl. Polym. Mater. 2021, 3, 5517−5526

recycling, which we will demonstrate in the last part of this contribution.

MATERIALS AND METHODS

Materials. Tetraethyl orthosilicate (TEOS, ≥99.0%), toluene (99.5%), and 2-propanol (99.5%) were purchased from Aldrich (Milwaukee, WI). Ammonium hydroxide solution (28−30%), triethylamine (TEA, 99.5%), and PE (medium density, MQ 200) were purchased from Sigma-Aldrich (St. Louis, MO). Ethanol (EtOH, absolute) for analysis was purchased from Merck (Darmstadt, Germany). Milli-Q water was produced by a Millipore Synergy system (Billerica, MA). Unless otherwise mentioned, all chemicals were used as received.

Stöber Synthesis of Silica Nanoparticles. SiO_2 NPs with a diameter of ∼110 nm were prepared by the Stöber method.[46] In a typical reaction, 168 mL of EtOH was mixed with 28 mL of Milli-Q water and 30 mL of TEOS in the presence of 2 mL of ammonium hydroxide in a round-bottom flask by stirring for 1.5 h at 500 rpm at room temperature. Subsequently, the SiO_2 NP dispersion was centrifuged at 10000 rpm for 30 min. Then, the collected SiO_2 NPs were redispersed in 2-propanol and centrifuged again. This washing step was repeated twice, followed by vacuum drying of the purified and collected SiO_2 NPs at room temperature for 12 h.

Silica Nanoparticle Characterization. A high-resolution scanning electron microscope (HR-TEM) (JEOL Field Emission JSM-7610F Plus, JEOL Benelux, Nieuw-Vennep, The Netherlands) was used to study the morphology of the SiO_2 NPs particles. The electron acceleration voltage was typically between 3 and 5 keV. Fourier transform infrared (FTIR) spectra were collected by a Bruker ALPHA single attenuated total reflection (ATR) FTIR spectrometer equipped with an ATR single reflection crystal (Bruker Optic GmbH, Ettlingen, Germany). The spectra were collected in the range 400−4000 cm^{-1} (spectral resolution of 4 cm^{-1}, 1280 scans). Background spectra were recorded against air. The as-prepared SiO_2 NPs were dispersed in water and toluene at a concentration of 2.5 wt % via intense sonication over 30 min. The hydrodynamic radius values of the particles in water and toluene were measured by dynamic light scattering (DLS) (Malvern Zetasizer Nano-ZS, Malvern Instruments, Malvern, UK).

Synthesis of Fluorescent Polyethylene Silica Nanocomposites in Air. We used two pathways to obtain FM containing PE, that is, in air and under an Ar atmosphere. First, we describe the preparative steps in air. We started with 0.4 g of 110 nm SiO_2 NPs, which were suspended in 10 mL of toluene in a round-bottom flask and exposed to 30 min intense sonication, followed by heating the suspension formed under vigorous stirring to 110 °C by immersing the flask in a thermostated oil bath. Simultaneously, 9.6 g of PE was dissolved in 30 mL of toluene by employing vigorous stirring in a round-bottom flask, which was immersed in a thermostated oil bath at 90 °C. Subsequently, the PE/toluene mixture was transferred to a reflux setup, followed by adding the SiO_2 NPs to the toluene suspension. After addition of the SiO_2 NPs suspension, the reaction mixture was refluxed at 110 °C for 24 h. Finally, the excess toluene was removed by drying the reaction mixture under a gentle nitrogen flow for 5 h. The PE/SiO_2 was dried to constant weight by vacuum drying at 40 °C for 24 h. This resulted in a PE/SiO_2 composite with a SiO_2 NP loading of 4 wt %. This composite is abbreviated as 4-PE/SiO_2. The same procedure was followed to produce 1.0 and 2.5 wt % PE/SiO_2 (1-PE/SiO_2 and 2.5-PE/SiO_2), in which 0.1 and 0.25 g of SiO_2 NPs and 9.9 and 9.75 g of PE were used, respectively. The amount of toluene used was not changed. Additionally, 4-PE/SiO_2 composites were prepared at 90 and 100 °C as well. (Unless otherwise mentioned, we refer to PE/SiO_2 prepared at 110 °C in the main text.) The pure PE sample was prepared by refluxing in toluene at 110 °C for 24 h and dried by using same procedure mentioned before as the control group.

Fluorescent Polyethylene Silica Nanocomposite Synthesis under Argon (Ar). To test the influence of air on the reaction and on the reaction products, for comparison, synthesis was also performed in Ar atmosphere. For this process 0.04 g of 110 nm SiO_2 NPs and 0.96 g of PE were dried in a vacuum oven at 40 °C for 48 h, and then the mixture was transferred into a 50 mL Schlenk tube with a magnetic stirring bar under a nitrogen environment (in a glovebox). Four milliliters of anhydrous toluene was added to the Schlenk tube. The Schlenk tube was sealed with a Teflon cap before it was removed from the glovebox. Next, the Schlenk tube was connected to a Schlenk line and flushed with Ar for10 min. Subsequently, the Schlenk tube was heated under vigorous stirring by a thermostated oil bath at 90 °C. After the PE was fully dissolved in the toluene, the Schlenk tube was disconnected from the Schlenk line and removed from the oil bath, followed by 15 min sonication in 90 °C water. After sonication, the Schlenk tube was reconnected to the Schlenk line under Ar and immersed into a thermostated oil bath at 110 °C. The reaction was allowed to proceed under Ar with vigorous stirring for 24 h. Next, the reaction mixture was extracted from the Schlenk tube and cooled in an ice bath, followed by drying under a gentle nitrogen flow for 5 h to remove the excess toluene. Finally, the PE/SiO_2 mixture was dried to constant weight by vacuum drying at 40 °C for 24 h.

Film Preparation. A hot press (Fontijne, The Netherlands) was used to press 200 μm thick PE/SiO_2 films in a stainless-steel mold (4 × 3 cm^2). The processing temperature, applied load, and press time were 110 °C, 200 kN, and 5 min, respectively.

Thin Film Characterization. An inverted Olympus IX71 fluorescence microscope equipped with an IX2-RFAC reflector turret filter cube (Olympus, Germany) and a PerkinElmer LS 55 fluorescence spectrometer (PerkinElmer, Waltham, MA) were used to study the optical properties of the PE/SiO_2 films. The filter cubes' excitation and emission cutoffs were 360−370 and 460 nm, respectively. The emission spectra were recorded by a fluorescence spectrometer with an excitation wavelength of 340, 360, and 380 nm. In addition, scanning electron microscopy (SEM) was performed by a JEOL Field Emission JSM-7610F Plus instrument (JEOL Benelux, Nieuw-Vennep, The Netherlands) to study the cross section of the PE/SiO_2 thin films. Before analysis, the thin films were freeze-fractured after cooling in liquid nitrogen for 15 min.

Carbon Quantum Dot Extraction. One gram of 4-PE/SiO_2 was dissolved in 10 mL of toluene thermostated at 90 °C in an oil bath. Following the complete dissolution of the 4-PE/SiO_2, the mixture was quenched into liquid nitrogen and left to cool to below ambient temperature for 15 min to avoid PE crystallization. Subsequently, the excess liquid nitrogen was removed, and the sample was left on the bench to heat slowly to room temperature. Next, the supernatant was filtered with a 200 nm pore size glass filter (Merck Millipore, USA) to remove the suspended agglomerated SiO_2 NPs, followed by collecting the CQDs by solvent removal of the filtrate via evaporation under a gentle nitrogen flow, which left a yellowish paste as residue for analysis.

Carbon Quantum Dot Characterization. Transmission electron microscopy (TEM) was performed by a FEI/Philips CM300 system (FEI, Eindhoven, The Netherlands). Diluted CQD dispersions in toluene were deposited on the carbon side of a carbon/copper grid (HC200-Cu) (EMS, Germany) before imaging. Images were obtained in the bright-field mode at a 300 kV acceleration voltage. Ultraviolet−visible (UV−vis) spectroscopy was performed by a LAMBDA 850 UV−vis spectrometer (PerkinElmer, Waltham, MA). The CQDs were dispersed in toluene via 10 min intense sonication. The CQD suspension was measured against pure toluene. The excitation and emission spectra were recorded by a PerkinElmer LS 55 fluorescence spectrometer (PerkinElmer, Waltham, MA) with an emission wavelength of 384 nm and excitation wavelengths of 286 and 340 nm.

Solution Blending. Twenty milligrams of CQDs (extracted) was solution blended with 180 mg of PE in 5 mL of toluene under vigorous stirring in a round-bottom flask while thermostated in an oil bath at 80 °C. After 30 min, the excess toluene was removed by drying the reaction mixture under a gentle nitrogen flow for 5 h. The PE/SiO_2 composite was dried to constant weight by vacuum drying at 40 °C for 24 h. The same procedure was used to blend 20 mg of 114 h thermally treated PE/SiO_2 (nonextracted) with 180 mg of PE. The as-

https://doi.org/10.1021/acsapm.1c00821
ACS Appl. Polym. Mater. 2021, 3, 5517−5526

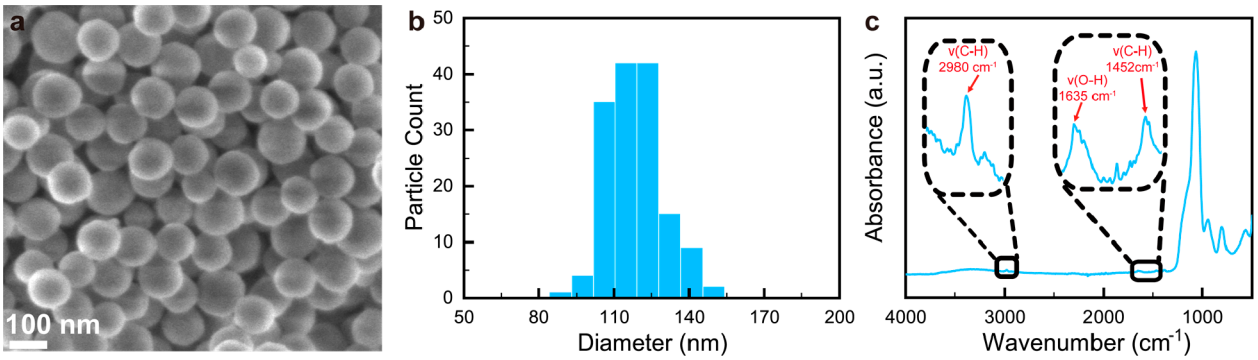

Figure 2. (a) SEM image and (b) size distribution of SiO_2 NPs used in this work. (c) Single reflection ATR-FTIR absorbance spectrum of the as-prepared SiO_2 NPs.

prepared nanocomposites were pressed to films (see section Film Preparation) and cut to different shapes before being observed under daylight and a 360 nm light source to identify the respective PE samples.

RESULTS AND DISCUSSION

SiO_2 NP Synthesis and Characterization. First, we employed a modified Stöber procedure to synthesize SiO_2 NPs.[46] Figures 2a and 2b show a SEM image and the size distribution of the SiO_2 NPs, respectively. The nearly spherical SiO_2 NPs have an average particle size of 114 ± 11 nm, and most of the particles have a diameter between 100 and 130 nm. Figure 2c shows a single reflection ATR-FTIR absorbance spectrum of the SiO_2 NPs. In the FTIR spectrum, the SiO_2 signature absorption bands ascribed to the asymmetric vibration of Si−O, the asymmetric vibration of Si−OH, and the symmetric vibration of Si−O are clearly observed at 1063, 940, and 803 cm^{-1}, respectively. The broad absorption band with a maximum at 3431 cm^{-1} and the small peak located at 1635 cm^{-1} are ascribed to O−H stretching absorbances by Si−OH bonds and to physically absorbed water.[47] The small absorption bands located at 2980 and 1452 cm^{-1} indicate the presence of CH_2/CH_3, which is attributed to residual ethoxy moieties.[47]

PE/SiO_2 Composites and Fluorescence Microscopy. In Figure 3, fluorescent microscope images (λ_{ex} 360−370 nm and

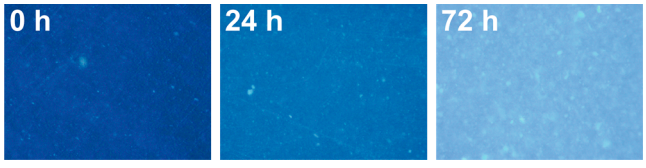

Figure 3. Fluorescent microscopy images of 2.5-PE/SiO_2 thin films prepared as a function of the reaction time up to 72 h in air.

λ_{em} > 460 nm) of 2.5-PE/SiO_2 thin films obtained by employing varying reaction times up to 72 h are shown. From this figure, it is clear that upon increasing the reaction time the observed fluorescence emission intensity increases (see also later). Additionally, for separate PE/toluene and SiO_2/toluene samples heated for 24 h in air at 110 °C, no fluorescence was observed. Thus, we conclude that the combination of SiO_2 NPs and PE together is required for the reaction that results in fluorescent material. In the following sections, we will first confirm that CQDs are formed and explain the role of the SiO_2 NPs in the reaction. In the last part of this work, we show that modest shifts in the emission wavelengths are obtained upon changing the reaction conditions (from air to Ar).

Origin of the Observed Fluorescence: CQD Isolation and Characterization. During preparation, as mentioned, liquid nitrogen quenching of the toluene solution containing 2.5-PE/SiO_2 and CQDs was used to suppress PE crystallization and leave the particles (SiO_2 NPs and CQDs) in the toluene phase. Following the removal of the residual PE and subsequently the SiO_2 NPs by filtration, the residual toluene fraction was dried to isolate the fluorophores. Subsequently, small quantities of a yellowish paste were formed at the bottom of the container. This paste was used to prepare samples for HR-TEM analysis. Figure 4a shows an HR-TEM image of the

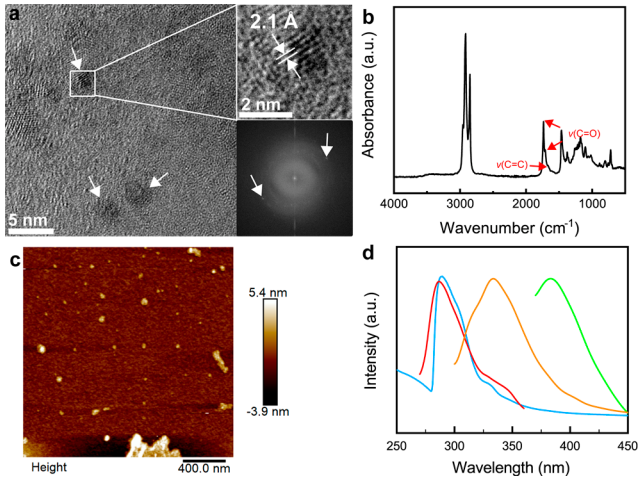

Figure 4. (a) HR-TEM image, (b) single reflection ATR-FTIR absorbance spectrum, and (c) AFM image. (d) Normalized UV−vis absorption (blue), excitation (λ_{em} = 386 nm) (red), and emission spectra (λ_{em} = 286 nm (orange) and 340 nm (green)) of the isolated CQDs and the polymeric residue suspended in toluene.

residual paste, revealing crystalline nanoparticles (dark, circular objects). The arrows in Figure 4a point at single fluorophores. From zoomed-in images (such as shown in the top right inset) and following a fast Fourier transform (FFT) analysis of the TEM intensities (bottom right inset), a lattice spacing of 2.1 Å for the nanoparticles was determined. This value agrees well with the (100) plane graphite lattice spacing typically observed for CQDs.[48−51] While we expected clear TEM images of the CQDs, the particle edges appear slightly blurred. We attribute this to the presence of residual polymer that the isolation process did not remove, combined with curvature effects. The

https://doi.org/10.1021/acsapm.1c00821
ACS Appl. Polym. Mater. 2021, 3, 5517−5526

residual polymer promoted particle agglomeration during TEM sample preparation. The average diameter for the CQDs was 2.3 ± 0.5 nm, which agrees with the particle height measured by AFM (2.2 ± 0.7 nm, see Figure 4c).

The residual polymer present and the fact that the samples for TEM imaging were retrieved as a yellowish paste point toward the presence of degraded polymer that remained in the toluene during liquid nitrogen quenching and was not removed by filtration and drying. Figure 4b shows an FTIR spectrum of the yellowish paste obtained. The spectrum has all the representative peaks of PE with additional peaks located at 1712 and 1736 cm^{-1} corresponding to absorbances of C═O from carboxylic acids and aldehyde, respectively.[52] Those peaks typically indicate thermooxidative degradation of PE.[53] There is also a noticeable small peak located at 1660 cm^{-1}, indicating that C═C bonds were also formed.[54] We note that as described in the literature, oxidation of PE is required for the formation of CQDs.[45] The sharp peak (289 nm) and the small shoulder (330−340 nm) from the UV−vis spectrum of the CQD suspension (Figure 4d) are ascribed to the $\pi-\pi^*$ transition of aromatic ring structures (C═C) and the $n-\pi^*$ transition of the oxidized groups (C═O), respectively.[55,56] The presence of C═C ($\pi-\pi^*$ transition) and C═O ($n-\pi^*$ transition) absorbance in the UV−vis spectrum are in agreement with the structures observed in the FTIR spectrum, shown in Figure 4b. The normalized excitation spectrum exhibits a peak and shoulder combination that is similar to the UV−vis spectrum. The excitation at 286 and 330−340 nm corresponds to the CQD core (aromatic ring structure) and surface defects (C═O containing groups).[57] The emission bands located at 337 and 383 nm are ascribed to the surface defects of CQDs. It is worth noting that when excited at 286 nm, the emission spectrum shows a small shoulder around 320 nm. This small shoulder is attributed to the photon emitted directly from the CQD cores without being trapped by surface defects.[58]

The absence of fluorescent and degradation products of PE heated without dispersed SiO_2 NPs confirms that the SiO_2 NPs play a role in forming the fluorescent CQDs. Therefore, to better understand the mechanism behind CQDs' formation during thermal treatment, one must first understand the role that the SiO_2 NPs play in the reaction, which we elucidate in the following section.

Role of SiO_2NPs in CQD Formation in Heated PE/SiO_2 Solutions. DLS was used to investigate the dispersion of the SiO_2 NPs in toluene. Additionally, the morphology of SiO_2 was observed by SEM in the PE matrix at room temperature. For DLS, the hydrodynamic radius of SiO_2NPs in water was also determined. Figures 5a and 5b show the hydrodynamic particle size of SiO_2 NPs suspended in water and in toluene, respectively.

The range of hydrodynamic particle diameter values of the SiO_2 NPs in water is around 110 ± 3 nm, which agrees with the determined dry particle size by SEM (Figure 2b). This confirms that after drying the SiO_2 NPs did not irreversibly aggregate. The hydrodynamic particle diameter values of the SiO_2 NPs in toluene, however, varied in the range of 750 ± 45 nm, which is nearly 7 times larger than the primary particle size, indicating severe particle agglomeration in toluene. Figure 6 shows SEM images of the cross sections of 1-, 2.5-, and 4-PE/SiO_2 films prepared after only 10 min of reaction time from the respective SiO_2 PE solutions. Figure 6 shows that almost all SiO_2 NPs are present as part of large agglomerates

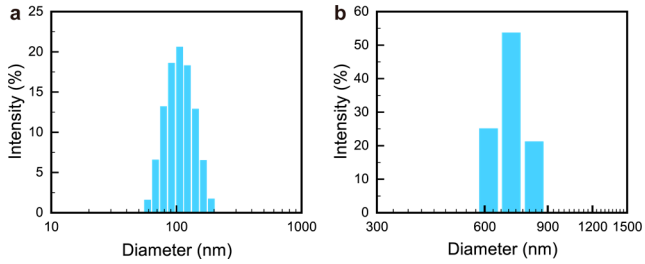

Figure 5. Hydrodynamic particle size of SiO_2 NPs dispersed in (a) water and (b) toluene.

(with sizes exceeding 1 μm) in 1- and 2.5-PE/SiO_2 films, while in the 4-PE/SiO_2 thin film, the observed SiO_2 NPs formed a large number of smaller agglomerates with a diameter in the submicrometer range. On the basis of these results, we conclude that the SiO_2 NPs agglomerated during the thermal treatment process. Like in mesoporous SiO_2 particles (aerogels), the silica agglomerates in the PE/toluene mixture have an open porous structure. According to the literature, these pores may act as nanometric size reactors that prolong the lifetime of radicals produced from the thermal degradation of polyolefins.[59] These long-lived radicals confined in the pores have more chance to react with other PE molecules, accelerating the thermal degradation of PE. The confinement effect on the kinetics of enzymatic reactions has been shown earlier by us and presumably can be extended to the radical activities of degraded PE.[60] Typically, the thermal degradation rate for PE is low at 110 °C.[61] When these nanometric-sized reactors are present, we increased the PE degradation reaction rate at lower temperatures and prepared CQDs from the degradation products within few hours.

Heat is a known physical factor that triggers the formation of macroradicals when accompanied by oxygen:[62]

$$RH + O_2 \rightarrow [RHO_2] \xrightarrow{\Delta} R^* + HO_2^*$$

RH represents the monomer units of PE (CH_2). Typically, the free radicals in solution at elevated temperature have a very short half-life time, in the range of 10^{-9} to 10^{-6} s. However, the pores/cavities accessible from the surface of SiO_2 NP agglomerates can act as nanometer-sized reaction vessels that prolong the half-life of free radicals and therefore accelerate the degradation of PE.[59] Consequently, the HO_2^* radicals formed in the nanocavities remain active for a longer time and have a higher chance of reacting with RH units to produce more R* radicals. Subsequently, the free radicals R* react with adjacent RH units to form vinyl groups resulting in chain scission and the formation of C═C bonds:

$$\sim C^*H-CH_2-CH_2\sim \rightarrow \sim CH{=}CH_2 + C^*H_2\sim$$

This mechanism is supported by the appearance of the observed C═C absorbance band at 1660 cm^{-1} in the FTIR spectrum (Figure 4b), indicating the presence of vinyl groups in CQDs and in the polymer residue.[63] During CQD formation, the initially degraded polymer forms C═C/C−C frameworks inside the porous agglomerated SiO_2 NPs during the thermal degradation/oxidation, thereby acting as skeletons/nucleus. As degradation progresses, these nuclei grow to nanometer-sized CQDs.[64]

Free radicals R* can also undergo oxidation with oxygen to form peroxide radicals (RO_2^*), followed by reacting with

https://doi.org/10.1021/acsapm.1c00821
ACS Appl. Polym. Mater. 2021, 3, 5517−5526

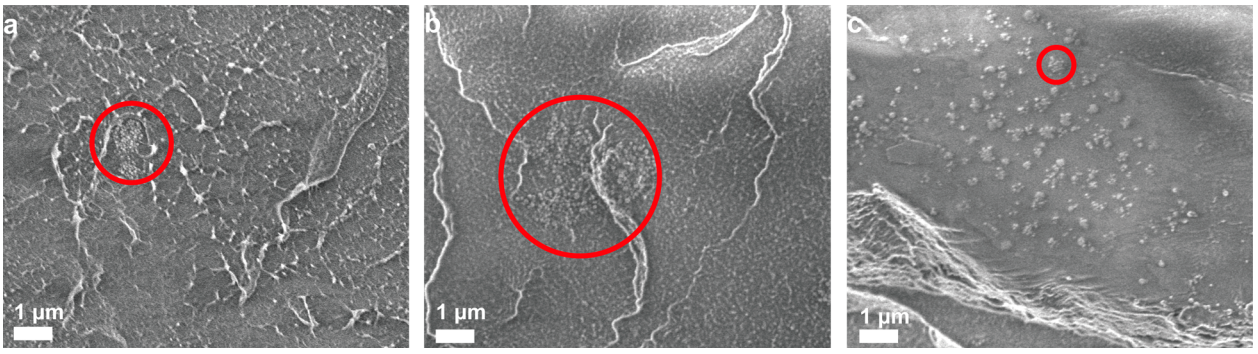

Figure 6. SEM images of cross-sectioned (a) 1-PE/SiO_2, (b) 2.5-PE/SiO_2, and (c) 4-PE/SiO_2 thin films after 10 min of thermal treatment. The red circles indicate SiO_2 NP agglomerates.

neighboring monomer units to form hydroperoxides (ROOH):[62]

$$R^* + O_2 \rightarrow RO_2^*$$

$$RO_2^* + RH \rightarrow ROOH + R^* \rightarrow ROH + RO^*$$

The presence of carboxylic acid (ROOH) and aldehyde (ROH) moieties formed by the thermal oxidation is also supported by the observed sharp peaks (C═O) located at 1712 and 1736 cm^{-1} in the FTIR spectrum (Figure 3), respectively. The formation of C═O can occur either on the CQDs, resulting in the presence of impurities and surface defects in the CQDs, or on the polymer chains, resulting in the formation of carbonyl groups. As it was not among the objectives of the scope of this study, we cannot confirm whether the CQDs do or do not have these defects. This requires more extensive purification and characterization of the CQDs.

Effect of SiO_2 NPs Concentration of Fluorescent Intensity of PE/SiO_2 Thin Films. To further investigate the influence of SiO_2 NPs on the fluorescent properties, PE/SiO_2 composites with particle concentrations of 1, 2.5, and 4 wt % were prepared with up to 24 h of thermal treatment at 110 °C in air. The as-prepared composites were processed into thin films and measured with a fluorescent microscope. Figure 7 shows the gray values of the fluorescence of 1-, 2.5-, and 4-PE/SiO_2 against reaction time. We note that the PE/SiO_2/toluene mixture needed the first 10 min to homogenize due to its high viscosity. As a consequence, 10 min is the first experimentally available reaction time for taking aliquots for further study. Furthermore, we note that the differences in baseline gray value intensities of the PE films with different SiO_2 NP loading (resulting from the differences in particle loading) lead to changes in the refraction of the excitation/emission light beams.

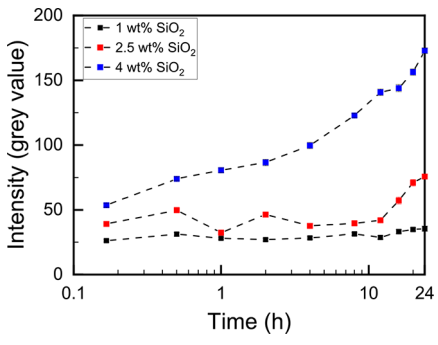

Figure 7. Gray value intensity of as-prepared 1-PE/SiO_2, 2.5-PE/SiO_2, and 4-PE/SiO_2 films as a function of the reaction time. The reaction was performed at 110 °C in air.

Interestingly, there is no significant change in the measured fluorescent intensity during the first few hours of the reaction for 1- and 2.5-PE/SiO_2. However, the fluorescent intensity gradually increases for the 4-PE/SiO_2 film right after the start of the reaction. In fact, for 1-PE/SiO_2 films, even after 24 h of thermal treatment, there is no noticeable change in the fluorescence intensity. However, the fluorescent intensity increased significantly for 2.5-PE/SiO_2 films after 8 h of thermal treatment.

This remarkable difference is explained by the relatively high concentration of SiO_2 agglomerates present in 4-PE/SiO_2 (Figure 6c). The increased amount of smaller SiO_2 agglomerates results in an increased specific contact area between the SiO_2 NPs and PE chains. Consequently, the relative number of accessible nanocavities to accelerate the CQD formation increases. For 1- and 2.5-PE/SiO_2, the relatively low particle surface area available for promoting the CQD formation results in a reduced rate of CQD formation. The observed dependence of CQD formation on the concentration and size of SiO_2 agglomerates confirms that the SiO_2 agglomerates play a crucial role in forming CQDs at relatively low temperatures and that their exploitation as an enabling platform in the facile synthesis of CQD-based FM is of interest for further exploration. For spectral engineering, we eventually need to be able to tune the emission wavelengths of the CQDs by varying the size of the emitters. The following sections show the first attempts to control the emission wavelengths of the CQDs and a proof of concept showing their potential as FMs in polymers to aid in sorting.

Fluorescent Spectra of PE/SiO_2 Thin Films and the Influence of the Reaction Temperature. In a first attempt to show the potential utilization of the CQDs as FMs, we examined their emission spectra as a function of particle concentration and reaction time upon excitation with 360 and 380 nm light, respectively. Figures 8a and 8b show the fluorescent emission spectra of 2.5- and 4-PE/SiO_2 thin films with an excitation wavelength of 360 and 380 nm, respectively.

The observed fluorescent emission maxima for the PE/SiO_2 samples fall into the blue emission range (380−500 nm), which is typically the result of the radiative recombination of e−h pairs in the sp^2 cluster and surface defects of CQDs.[65] A clear red-shift of a few nanometers in the fluorescent emission is observed in the fluorescent spectra by increasing the

https://doi.org/10.1021/acsapm.1c00821
ACS Appl. Polym. Mater. 2021, 3, 5517−5526

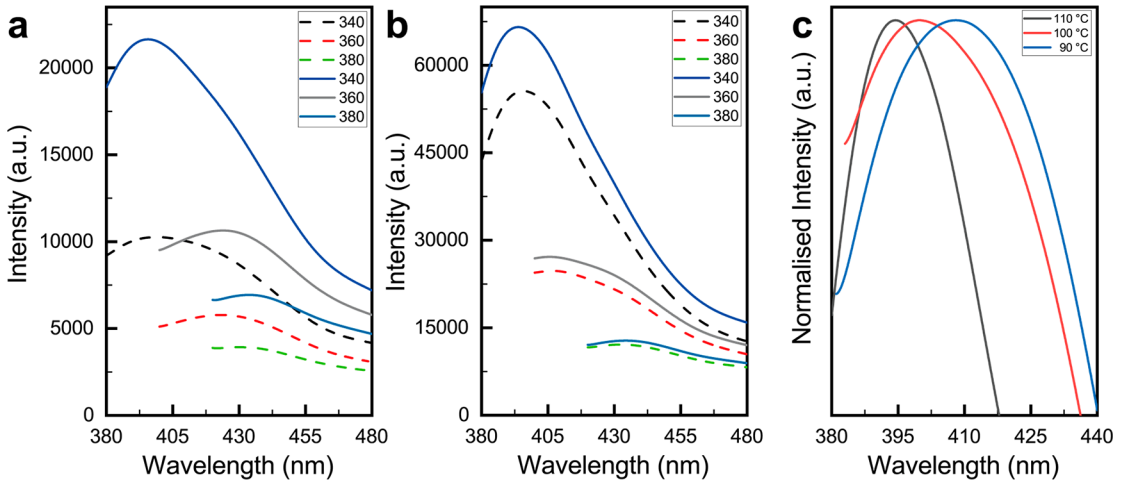

Figure 8. Fluorescent emission spectra of (a) 2.5-PE/SiO_2 and (b) 4-PE/SiO_2 thin films prepared in air with 20 h (dashed lines) and 24 h (solid lines) reaction times upon excitation with 340, 360, and 380 nm wavelengths. (c) Fluorescent emission spectra of thin films of 4-PE/SiO_2 upon excitation with 340 nm light, fabricated at reaction temperatures of 90, 100, and 110 °C for 24 h in air.

excitation wavelength from 340 to 380 nm. Although the exact mechanism for CQDs fluorescent emission is still under debate, it is generally agreed that the CQDs' size and surface status significantly influence the fluorescent properties of CQDs.[66] We consider that the excitation-dependent fluorescence behavior of our thin films is a combination of CQDs size dispersity, impurities, and surface defects.[67] Furthermore, a modest red-shift was also observed in the fluorescent emission spectrum when the reaction time increased from 20 to 24 h. The observed red-shift can be tentatively explained by the longer time available for the CQDs to grow, resulting in larger CQDs that typically have a red-shift in their emission spectrum.[43]

Figure 8c shows normalized fluorescent emission spectra of 4-PE/SiO_2 samples fabricated at different temperatures. One can observe in Figure 8c that upon increasing the reaction temperature from 90 to 110 °C for the 4-PE/SiO_2 mixture the emission peak shifts from 408 to 394 nm upon excitation with 340 nm light. It is known that upon increasing the reaction temperature the oxygen solubility decreases.[68] Therefore, it is reasonable to assume that upon increasing the reaction temperature from 90 to 110 °C fewer oxygen molecules were present in the reaction mixture, which reduced the chance for free radicals to be involved in oxidation reactions and the formation of C═O species. This could decrease the number of surface traps and impurities (C═O) present in the formed CQDs leading to less energy loss for the fluorescent emission, resulting in higher emission energy for the CQDs prepared at higher temperatures.[69]

To further elucidate the role oxygen during the CQD synthesis, the reaction was performed in an Ar atmosphere for 4-PE/SiO_2 mixtures at 110 °C. The corresponding fluorescent excitation and emission spectra of the 4-PE/SiO_2 samples are shown in Figure 9. The maximum excitations for 4-PE/SiO_2 synthesized in air and Ar are located at 240 and 260 nm, respectively. These excitation peaks are ascribed to the photon absorption of C═C (aromatic structure) in the CQD core.[70] The corresponding emission centers are located at 350 and 285 nm.[57] The blue-shift in emission wavelength upon substituting air with Ar is ascribed to the reduced presence of surface defects (surface oxidation) of the CQDs when prepared without the presence of oxygen. This means that the

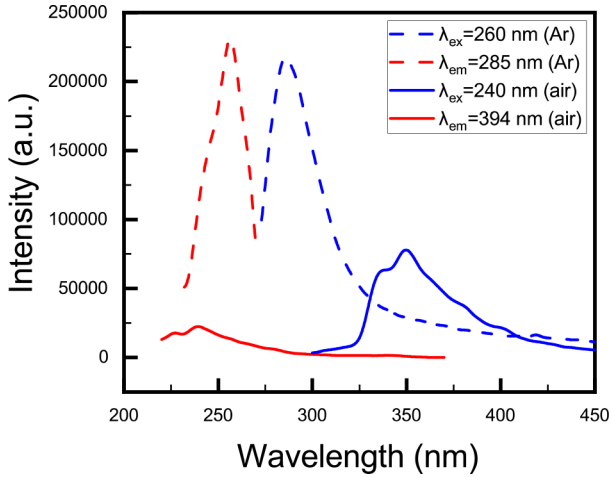

Figure 9. Fluorescent excitation and emission spectra of 4-PE/SiO_2 thin films prepared with 24 h reaction time in air (solid line) and Ar (dashed line) atmosphere.

photons are directly emitted from the aromatic ring structure (C═C) upon excitation and that without the presence of surface defects to trap these photons they can maintain a higher energy level, therefore emitting at a shorter wavelength.[58]

Overall, these results demonstrate that with minor modifications to the reaction conditions changes in the CQD emissions are accessible, rendering our system a valuable designer platform for the controlled synthesis of PE-based FMs at mild reaction conditions.

Solution Blending CQDs and PE/SiO_2 with Pure PE. We used solution blending to prepare CQD containing PE films to demonstrate the applicability of the CQD as fluorescent markers in virgin polymers. As-prepared CQD 4-PE/SiO_2 (114 h reaction at 110 °C in air) and isolated CQDs (extracted from 4-PE/SiO_2 after 24 h reaction in air) were used as tracer batches to prepare PE films with a tracer loading of 10 wt % (meaning the actual CQD concentration is unknown). Following compression molding, film samples were cut to easily recognizable shapes, i.e., circles and triangles, respectively. In addition, pristine PE films were prepared and

https://doi.org/10.1021/acsapm.1c00821
ACS Appl. Polym. Mater. 2021, 3, 5517−5526

cut to rectangular shapes for comparison. Five pieces were placed together from each PE film type, and photos were taken in daylight (Figure 10a) and upon excitation with 360 nm light (Figure 10b).

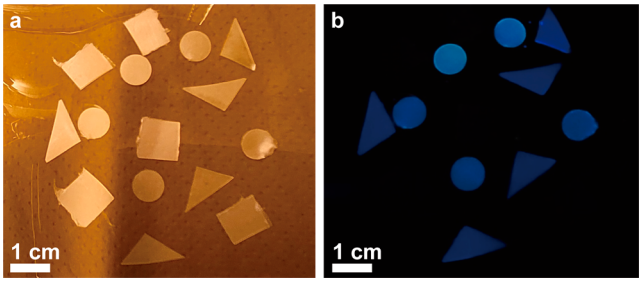

Figure 10. Photos of pure PE (rectangles), PE/CQD (triangles), and CQD 4-PE/SiO_2 (circles) films in (a) daylight and (b) upon excitation with 367 nm light.

In Figure 10a (photo taken in daylight), all pieces are visible and their shape is clearly identifiable. Upon excitation with 367 nm light, only the CQD-loaded pieces are visible by their emission in the blue range. The color difference (not intensity) between triangular (darker blue) and circular (lighter blue) pieces under 367 nm excitation is due to differences in thermal treatment time, resulting in the presence of larger CQDs in the circular PE films, as discussed earlier. The observed modest red-shift is in agreement with this observation.[43] Also, from this simple visual experiment, we learn that the embedded SiO_2 NPs do not affect the PE samples' detectability. Overall, we conclude that the simple preparation method at mild reaction conditions of CQD FMs in SiO_2/PE mixtures described here is a promising approach for fluorescence marking. Further in-depth exploration to enhance the CQD traceability is needed and is underway to explain details of the fluorescence. In addition, upon expanding the variations and control of emission wavelengths, our simple preparation method without requiring extensive purification methods opens a broad range of novel applications, e.g., counterfeiting, sorting, tracing, etc.

CONCLUSIONS

PE containing CQDs markers with tunable fluorescence was prepared by a facile thermal approach operated at mild conditions. For the reaction employed, solvent-induced SiO_2 NP aggregation provided surface-exposed nanocavities that were assumed to function as nanoreactors, enabling CQDs to form at relatively low reaction temperatures. TEM imaging of isolated CQD particles, UV spectroscopy, and fluorescent measurements confirmed the successful preparation of CQDs. The emission maximum for PE/CQD samples was tunable between 394 and 408 nm by decreasing the reaction temperature from 110 to 90 °C. PE/CQD samples prepared in the absence of oxygen only emitted in the ultraviolet region (286 nm). Finally, we successfully exploited CQDs with a different emission maximum as FMs in PE compression molded films. Upon irradiating with 367 nm light, the different PE samples were readily visually identified.

ASSOCIATED CONTENT

Supporting Information

The Supporting Information is available free of charge at https://pubs.acs.org/doi/10.1021/acsapm.1c00821.

Non-normalized emission spectra of CQDs suspension with excitation wavelength of 340 and 360 nm, non-normalized emission spectra of CQDs suspension with 0, 10, and 30 min sonication, and wide-area TEM image of CQDs (PDF)

AUTHOR INFORMATION

Corresponding Authors

G. Julius Vancso − *Sustainable Polymer Chemistry and Materials Science and Technology of Polymers, MESA+ Institute for Nanotechnology, University of Twente, 7500AE Enschede, The Netherlands;* orcid.org/0000-0003-4718-0507; Email: g.j.vancso@utwente.nl

Joost Duvigneau − *Sustainable Polymer Chemistry and Materials Science and Technology of Polymers, MESA+ Institute for Nanotechnology, University of Twente, 7500AE Enschede, The Netherlands;* orcid.org/0000-0002-2810-2768; Email: j.duvigneau@utwente.nl

Author

Sida Yin − *Sustainable Polymer Chemistry and Materials Science and Technology of Polymers, MESA+ Institute for Nanotechnology, University of Twente, 7500AE Enschede, The Netherlands*

Complete contact information is available at: https://pubs.acs.org/10.1021/acsapm.1c00821

Funding

This work was funded by the Interreg V project Druckbare RFID-Tags für Massenmärkte (DruIDe), MESA+ Institute for Nanotechnology, and University of Twente.

Notes

The authors declare no competing financial interest.

ACKNOWLEDGMENTS

This work was funded as part of the Interreg V project Druckbare RFID-Tags für Massenmärkte (DruIDe) and by the University of Twente. The authors thank Dr. Hubert Gojzewski for the help with conducting AFM measurements. The authors also acknowledge M.S.c. Min Lin for her help with UV−vis microscopy measurements.

REFERENCES

(1) Ruj, B.; Pandey, V.; Jash, P.; Srivastava, V. K. Sorting of Plastic Waste for Effective Recycling. *Int. J. Appl. Sci. Eng. Res.* **2015**, *4* (4), 564−571.

(2) Ragaert, K.; Delva, L.; van Geem, K. Mechanical and Chemical Recycling of Solid Plastic Waste. *Waste Manage.* **2017**, *69*, 24−58.

(3) Singh, N.; Hui, D.; Singh, R.; Ahuja, I. P. S.; Feo, L.; Fraternali, F. Recycling of Plastic Solid Waste: A State of Art Review and Future Applications. *Composites, Part B* **2017**, *115*, 409−422.

(4) Pol, V. G.; Thiyagarajan, P. Remediating Plastic Waste into Carbon Nanotubes. *J. Environ. Monit.* **2010**, *12* (2), 455−459.

(5) Müller, R. J.; Kleeberg, I.; Deckwer, W. D. Biodegradation of Polyesters Containing Aromatic Constituents. *J. Biotechnol.* **2001**, *86* (2), 87−95.

(6) Manfredi, S.; Tonini, D.; Christensen, T. H.; Scharff, H. Landfilling of Waste: Accounting of Greenhouse Gases and Global Warming Contributions. *Waste Manage. Res.* **2009**, *27* (8), 825−836.

(7) Rhodes, C. J. Plastic Pollution and Potential Solutions. *Sci. Prog.* **2018**, *101* (3), 207−260.

(8) Tall, S. (2000). Recycling of Mixed Plastic Waste − Is Separation Worthwhile? Royal Institute of Technology. https://www.

diva-portal.org/smash/get/diva2:8665/FULLTEXT01.pdf (accessed 2021-09-19).
(9) Geyer, R.; Jambeck, J. R.; Law, K. L. Production, Use, and Fate of All Plastics Ever Made. *Sci. Adv.* **2017**, *3* (7), e1700782.
(10) Verma, R.; Vinoda, K. S.; Papireddy, M.; Gowda, A. N. S. Toxic Pollutants from Plastic Waste- A Review. *Procedia Environ. Sci.* **2016**, *35*, 701−708.
(11) Johnke, B. Emissions From Waste Incineration. In *Good Practice Guidance and Uncertainty Management in National Greenhouse Gas Inventories*; Intergovernmental Panel on Climate Change, 2000; pp 455−468. https://www.ipcc-nggip.iges.or.jp/public/gp/english/ (accessed on 2021-09-19).
(12) Hopewell, J.; Dvorak, R.; Kosior, E. Plastics Recycling: Challenges and Opportunities. *Philos. Trans. R. Soc., B* **2009**, *364* (1526), 2115−2126.
(13) Ross, S.; Evans, D. The Environmental Effect of Reusing and Recycling a Plastic-Based Packaging System. *J. Cleaner Prod.* **2003**, *11* (5), 561−571.
(14) Taranic, I.; Behrens, A.; Corrado, T. Understanding the Circular Economy in Europe from Resource Efficiency to Sharing Platforms: the CEPS Framework. *CEPS Special Reports* **2016**, *143*, 29.
(15) Wang, C.; Wang, H.; Fu, J.; Liu, Y. Flotation Separation of Waste Plastics for Recycling-A Review. *Waste Manage.* **2015**, *41*, 28−38.
(16) Reinsch, E.; Frey, A.; Albrecht, V.; Simon, F.; Peuker, U. Continuous Electric Sorting in the Recycling Process of Plastics. *Chem. Ing. Technol.* **2014**, *86*, 784−796.
(17) Dong, J.; Zhang, P.; Wang, W.; Li, J.; Chen, G. An Experimental Study on Performance and Structural Improvements of a Novel Elutriator. *Processes* **2021**, *9*, 478.
(18) Censori, M.; La Marca, F.; Carvalho, M. T. Separation of Plastics: The Importance of Kinetics Knowledge in the Evaluation of Froth Flotation. *Waste Manage.* **2016**, *54*, 39−43.
(19) Thiounn, T.; Smith, R. C. Advances and Approaches for Chemical Recycling of Plastic Waste. *J. Polym. Sci.* **2020**, *58* (10), 1347−1364.
(20) Al-Salem, S. M.; Lettieri, P.; Baeyens, J. Recycling and Recovery Routes of Plastic Solid Waste (PSW): A Review. *Waste Manage.* **2009**, *29* (10), 2625−2643.
(21) Brunner, S.; Fomin, P.; Kargel, C. Automated Sorting of Polymer Flakes: Fluorescence Labeling and Development of a Measurement System Prototype. *Waste Manage.* **2015**, *38* (1), 49−60.
(22) Maris, E.; Aoussat, A.; Naffrechoux, E.; Froelich, D. Polymer Tracer Detection Systems with UV Fluorescence Spectrometry to Improve Product Recyclability. *Miner. Eng.* **2012**, *29*, 77−88.
(23) Massardier, V.; Louizi, M.; Maris, E.; Froelich, D. High Shear Dispersion of Tracers in Polyolefins for Improving Their Detection. *Polim.: Cienc. Tecnol.* **2015**, *25* (5), 466−476.
(24) Ahmad, S. R. A New Technology for Automatic Identification and Sorting of Plastics for Recycling. *Environ. Technol.* **2004**, *25* (10), 1143−1149.
(25) Langhals, H.; Zgela, D.; Schlücker, T. High Performance Recycling of Polymers by Means of Their Fluorescence Lifetimes. *Green Sustainable Chem.* **2014**, *04* (03), 144−150.
(26) Gao, G.; Turshatov, A.; Howard, I. A.; Busko, D.; Joseph, R.; Hudry, D.; Richards, B. S. Up-Conversion Fluorescent Labels for Plastic Recycling: A Review. *Adv. Sustainable Syst.* **2017**, *1* (5), 1600033.
(27) Arenas-Vivo, A.; Beltrán, F. R.; Alcázar, V.; de la Orden, M. U.; Martinez Urreaga, J. Fluorescence Labeling of High Density Polyethylene for Identification and Separation of Selected Containers in Plastics Waste Streams. Comparison of Thermal and Photochemical Stability of Different Fluorescent Tracers. *Mater. Today Commun.* **2017**, *12* (July), 125−132.
(28) Woidasky, J.; Sander, I.; Schau, A.; Moesslein, J.; Wendler, P.; Wacker, D.; Gao, G.; Kirchenbauer, D.; Kumar, V.; Busko, D.; Howard, I. A.; Richards, B. S.; Turshatov, A.; Wiethoff, S.; Lang-Koetz, C. Inorganic Fluorescent Marker Materials for Identification of Post-Consumer Plastic Packaging. *Resour., Conserv. Recycl.* **2020**, *161*, 104976.
(29) Field, M. S.; Wilhelm, R. G.; Quinlan, J. F.; Aley, T. J. An Assessment of the Potential Adverse Properties of Fluorescent Tracer Dyes Used for Groundwater Tracing. *Environ. Monit. Assess.* **1995**, *38* (1), 75−96.
(30) Tchounwou, P. B.; Yedjou, C. G.; Patlolla, A. K.; Sutton, D. J. Heavy Metal Toxicity and the Environment. *EXS* **2012**, *101*, 133−164.
(31) Ali, H.; Khan, E.; Ilahi, I. Environmental Chemistry and Ecotoxicology of Hazardous Heavy Metals: Environmental Persistence, Toxicity, and Bioaccumulation. *J. Chem.* **2019**, *2019*, 6730305.
(32) Alford, R.; Simpson, H. M.; Duberman, J.; Hill, G. C.; Ogawa, M.; Regino, C.; Kobayashi, H.; Choyke, P. L. Toxicity of Organic Fluorophores Used in Molecular Imaging: Literature Review. *Mol. Imaging* **2009**, *8* (6), 341−354.
(33) Molaei, M. J. Principles, Mechanisms, and Application of Carbon Quantum Dots in Sensors: A Review. *Anal. Methods* **2020**, *12* (10), 1266−1287.
(34) Zhang, Z.; Zhang, J.; Chen, N.; Qu, L. Graphene Quantum Dots: An Emerging Material for Energy-Related Applications and Beyond. *Energy Environ. Sci.* **2012**, *5* (10), 8869−8890.
(35) Shen, J.; Zhu, Y.; Yang, X.; Li, C. Graphene Quantum Dots: Emergent Nanolights for Bioimaging, Sensors, Catalysis and Photovoltaic Devices. *Chem. Commun.* **2012**, *48* (31), 3686−3699.
(36) Zheng, X. T.; Ananthanarayanan, A.; Luo, K. Q.; Chen, P. Glowing Graphene Quantum Dots and Carbon Dots: Properties, Syntheses, and Biological Applications. *Small* **2015**, *11* (14), 1620−1636.
(37) Zhou, J.; Booker, C.; Li, R.; Zhou, X.; Sham, T. K.; Sun, X.; Ding, Z. An Electrochemical Avenue to Blue Luminescent Nanocrystals from Multiwalled Carbon Nanotubes (MWCNTs). *J. Am. Chem. Soc.* **2007**, *129* (4), 744−745.
(38) Sun, Y. P.; Zhou, B.; Lin, Y.; Wang, W.; Fernando, K. A. S.; Pathak, P.; Meziani, M. J.; Harruff, B. A.; Wang, X.; Wang, H.; Luo, P. G.; Yang, H.; Kose, M. E.; Chen, B.; Veca, L. M.; Xie, S. Y. Quantum-Sized Carbon Dots for Bright and Colorful Photoluminescence. *J. Am. Chem. Soc.* **2006**, *128* (24), 7756−7757.
(39) Huang, H.; Xu, Y.; Tang, C. J.; Chen, J. R.; Wang, A. J.; Feng, J. J. Facile and Green Synthesis of Photoluminescent Carbon Nanoparticles for Cellular Imaging. *New J. Chem.* **2014**, *38* (2), 784−789.
(40) Sharma, A.; Das, J. Small Molecules Derived Carbon Dots: Synthesis and Applications in Sensing, Catalysis, Imaging, and Biomedicine. *J. Nanobiotechnol.* **2019**, *17* (1), 92.
(41) Hu, Y.; Gao, Z.; Yang, J.; Chen, H.; Han, L. Environmentally Benign Conversion of Waste Polyethylene Terephthalate to Fluorescent Carbon Dots for "On-Off-On" Sensing of Ferric and Pyrophosphate Ions. *J. Colloid Interface Sci.* **2019**, *538*, 481−488.
(42) Hu, Y.; Yang, J.; Tian, J.; Jia, L.; Yu, J. S. Green and Size-Controllable Synthesis of Photoluminescent Carbon Nanoparticles from Waste Plastic Bags. *RSC Adv.* **2014**, *4* (88), 47169−47176.
(43) Wang, Y.; Hu, A. Carbon Quantum Dots: Synthesis, Properties and Applications. *J. Mater. Chem. C* **2014**, *2* (34), 6921−6939.
(44) Wang, X.; Feng, Y.; Dong, P.; Huang, J. A Mini Review on Carbon Quantum Dots: Preparation, Properties, and Electrocatalytic Application. *Front. Chem. (Lausanne, Switz.)* **2019**, *7*, 671.
(45) Huang, C.; Dong, H.; Su, Y.; Wu, Y.; Narron, R.; Yong, Q. Synthesis of Carbon Quantum Dot Nanoparticles Derived from Byproducts in Bio-Refinery Process for Cell Imaging and in Vivo Bioimaging. *Nanomaterials* **2019**, *9* (3), 387.
(46) Stöber, W.; Fink, A.; Bohn, E. Controlled Growth of Monodisperse Silica Spheres in the Micron Size Range. *J. Colloid Interface Sci.* **1968**, *26* (1), 62−69.
(47) Beganskiene, A.; Sirutkaitis, V.; Kurtinaitiene, M.; Juskenas, R.; Kareiva, A. FTIR, TEM and NMR Investigations of Stöber Silica Nanoparticles. *Mater. Sci.* **2004**, *10* (4), 287−290.
(48) Dager, A.; Uchida, T.; Maekawa, T.; Tachibana, M. Synthesis and Characterization of Mono-Disperse Carbon Quantum Dots from

Fennel Seeds: Photoluminescence Analysis Using Machine Learning. *Sci. Rep.* **2019**, *9* (1), 1−12.
(49) Yang, H.; Liu, Y.; Guo, Z.; Lei, B.; Zhuang, J.; Zhang, X.; Liu, Z.; Hu, C. Hydrophobic Carbon Dots with Blue Dispersed Emission and Red Aggregation-Induced Emission. *Nat. Commun.* **2019**, *10* (1), 1−11.
(50) Lu, S.; Xiao, G.; Sui, L.; Feng, T.; Yong, X.; Zhu, S.; Li, B.; Liu, Z.; Zou, B.; Jin, M.; Tse, J. S.; Yan, H.; Yang, B. Piezochromic Carbon Dots with Two-Photon Fluorescence. *Angew. Chem.* **2017**, *129* (22), 6283−6287.
(51) Wang, T. Y.; Chen, C. Y.; Wang, C. M.; Tan, Y. Z.; Liao, W. S. Multicolor Functional Carbon Dots via One-Step Refluxing Synthesis. *ACS Sens.* **2017**, *2* (3), 354−363.
(52) Hamid, S. H. *Handbook of Polymer Degradation*; CRC Press: 2000.
(53) Gardette, M.; Perthue, A.; Gardette, J. L.; Janecska, T.; Földes, E.; Pukánszky, B.; Therias, S. Photo- and Thermal-Oxidation of Polyethylene: Comparison of Mechanisms and Influence of Unsaturation Content. *Polym. Degrad. Stab.* **2013**, *98* (11), 2383−2390.
(54) Vogel, C.; Morita, S.; Sato, H.; Noda, I.; Ozaki, Y.; Siesler, H. W. Thermal Degradation of Poly(3-Hydroxybutyrate) and Poly(3-Hydroxybutyrate- Co-3-Hydroxyhexanoate) in Nitrogen and Oxygen Studied by Thermogravimetric- Fourier Transform Infrared Spectroscopy. *Appl. Spectrosc.* **2007**, *61* (7), 755−764.
(55) Sun, X.; Lei, Y. Fluorescent Carbon Dots and Their Sensing Applications. *TrAC, Trends Anal. Chem.* **2017**, *89*, 163−180.
(56) Ahn, J.; Song, Y.; Kwon, J. E.; Lee, S. H.; Park, K. S.; Kim, S.; Woo, J.; Kim, H. Food Waste-Driven N-Doped Carbon Dots: Applications for Fe3+ Sensing and Cell Imaging. *Mater. Sci. Eng., C* **2019**, *102*, 106−112.
(57) Dhenadhayalan, N.; Lin, K. C.; Suresh, R.; Ramamurthy, P. Unravelling the Multiple Emissive States in Citric-Acid-Derived Carbon Dots. *J. Phys. Chem. C* **2016**, *120* (2), 1252−1261.
(58) Arumugam, S. S.; Xuing, J.; Viswadevarayalu, A.; Rong, Y.; Sabarinathan, D.; Ali, S.; Agyekum, A. A.; Li, H.; Chen, Q. Facile Preparation of Fluorescent Carbon Quantum Dots from Denatured Sour Milk and Its Multifunctional Applications in the Fluorometric Determination of Gold Ions, in Vitro Bioimaging and Fluorescent Polymer Film. *J. Photochem. Photobiol., A* **2020**, *401*, 112788.
(59) Sakata, Y.; Uddin, M. A.; Muto, A. Degradation of Polyethylene and Polypropylene into Fuel Oil by Using Solid Acid and Non-Acid Catalysts. *J. Anal. Appl. Pyrolysis* **1999**, *51* (1), 135−155.
(60) Chen, Q.; Schönherr, H.; Vancso, G. J. Block-Copolymer Vesicles as Nanoreactors for Enzymatic Reactions. *Small* **2009**, *5* (12), 1436−1445.
(61) Yang, R.; Liu, Y.; Yu, J.; Wang, K. Thermal Oxidation Products and Kinetics of Polyethylene Composites. *Polym. Degrad. Stab.* **2006**, *91* (8), 1651−1657.
(62) Shibryaeva, L. Thermal Oxidation of Polypropylene and Modified Polypropylene - Structure Effects. *Polypropylene* **2012**, 63−86.
(63) Iring, M.; Földes, E.; Barabás, K.; Kelen, T.; Tüdős, F.; Ódor, L. Thermal Oxidation of Linear Low Density Polyethylene. *Polym. Degrad. Stab.* **1986**, *14* (4), 319−332.
(64) He, M.; Zhang, J.; Wang, H.; Kong, Y.; Xiao, Y.; Xu, W. Material and Optical Properties of Fluorescent Carbon Quantum Dots Fabricated from Lemon Juice via Hydrothermal Reaction. *Nanoscale Res. Lett.* **2018**, *13* (1), 175.
(65) Zhu, C.; Yang, S.; Wang, G.; Mo, R.; He, P.; Sun, J.; Di, Z.; Kang, Z.; Yuan, N.; Ding, J.; Ding, G.; Xie, X. A New Mild, Clean and Highly Efficient Method for the Preparation of Graphene Quantum Dots Without By-Products. *J. Mater. Chem. B* **2015**, *3* (34), 6871−6876.
(66) Zhu, S.; Song, Y.; Zhao, X.; Shao, J.; Zhang, J.; Yang, B. The Photoluminescence Mechanism in Carbon Dots (Graphene Quantum Dots, Carbon Nanodots, and Polymer Dots): Current State and Future Perspective. *Nano Res.* **2015**, *8* (2), 355−381.
(67) Cayuela, A.; Soriano, M. L.; Carrillo-Carrión, C.; Valcárcel, M. Semiconductor and Carbon-Based Fluorescent Nanodots: the Need for Consistency. *Chem. Commun.* **2016**, *52* (7), 1311−1326.
(68) Li, A.; Tang, S.; Tan, P.; Liu, C.; Liang, B. Measurement and Prediction of Oxygen Solubility in Toluene at Temperatures from 298.45 to 393.15 K and Pressures up to 1.0 MPa. *J. Chem. Eng. Data* **2007**, *52* (6), 2339−2344.
(69) Zhang, R.; Adsetts, J. R.; Nie, Y.; Sun, X.; Ding, Z. Electrochemiluminescence of Nitrogen- and Sulfur-Doped Graphene Quantum Dots. *Carbon* **2018**, *129*, 45−53.
(70) Sharma, A.; Gadly, T.; Neogy, S.; Ghosh, S. K.; Kumbhakar, M. Molecular Origin and Self-Assembly of Fluorescent Carbon Nanodots in Polar Solvents. *J. Phys. Chem. Lett.* **2017**, *8* (5), 1044−1052.

https://doi.org/10.1021/acsapm.1c00821
ACS Appl. Polym. Mater. 2021, 3, 5517−5526